# Self-Powered Inhomogeneous Strain Sensor Enabled Joint Motion and Three-Dimensional Muscle Sensing

Haiming Wang,[†,‡,∥] Ding Li,[†,‡,∥] Wei Zhong,[†,‡,∥] Liang Xu,[†,‡] Tao Jiang,[†,‡] and Zhong Lin Wang*[,†,‡,§]

[†]Beijing Key Laboratory of Micro−Nano Energy and Sensor, Beijing Institute of Nanoenergy and Nanosystems, Chinese Academy of Sciences, Beijing 100083, P. R. China
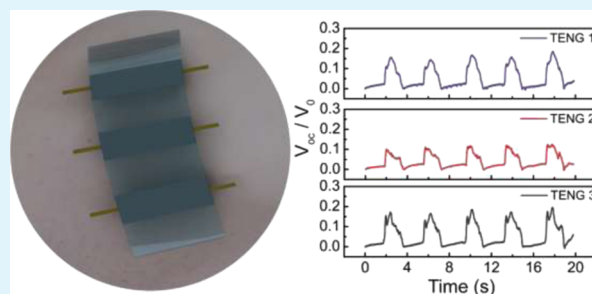
[‡]School of Nanoscience and Technology, University of Chinese Academy of Sciences, Beijing 100049, P. R. China

[§]School of Materials Science and Engineering, Georgia Institute of Technology, Atlanta, Georgia 30332, United States

**S** Supporting Information

**ABSTRACT:** Wearable electronics containing different functional sensors with abilities to meet people's daily needs are highly desirable. Here, a stretchable triboelectric nanogenerator (TENG) for wearable electronics is demonstrated. By stacking two layers of silicone rubbers embedded with silver nanowires (AgNWs) and a Ni foam as electrodes, respectively, the fabricated TENG can serve as a new type of sensor that is wearable, stretchable, skin-friendly, noninvasive, and durable. It can convert mechanical deformation into electric signals. Deformation like stretching and extruding of the TENG results in interlayer rubbing because of inhomogeneous strain, producing triboelectric charges that can induce voltage signals in the electrodes in response to the deformation. On the basis of the principle, a joint sensor based on the TENG is demonstrated, which can generate different output voltages according to the bending degrees of the joint. Furthermore, a three-dimensional sensor integrating three TENGs is fabricated to depict the deformations of different muscle areas. The output voltages of the three TENGs can be simultaneously monitored to reflect the deformation degrees of different muscle areas.



**KEYWORDS:** triboelectric nanogenerator, inhomogeneous strain, wearable electronics, three-dimensional sensor, muscle sensing

## INTRODUCTION

Nowadays, ubiquitous portable electronics have gradually entered into people's daily lives and greatly changed people's lifestyle. Wearable electronics as emerging intelligent devices are expected to be transparent,[1] stretchable,[2] biocompatible,[3] and foldable,[4] which can be conformally[5] attached to an uneven surface comparing to today's brittle and rigid electronics. With the improvement of human living standards, wearable electronics play a more and more significant role in health monitoring,[6] big data collecting,[7] soft robotics,[8] and virtual reality.[9] Unlike implantable electronics,[10] wearable electronics are much easier to implement and will not fail over weeks or months with the degradation of signals.[11] Therefore, wearable electronics are much easier to access in our daily lives.[12] Today's wearable electronics are still in the early stage, with two big accompanying challenges. On one hand, silicon[13] or metal materials[14] with high elastic moduli are still largely used in wearable electronics, resulting in a mechanical mismatch between electronics and a biological interface.[15] Thus, it is important to develop suitable materials with appropriate elastic moduli.[16] On the other hand, today's wearable electronics mostly depend on an external power source, like lithium batteries,[17] capacitors,[18] and so on,[19] which means it is necessary to replace or charge them regularly when they run out of power. A lot of manpower and resources will be consumed to maintain

these wearable electronics working daily.[20] This is almost impossible in this era of Internet of Things.

Triboelectric nanogenerators (TENGs), first invented in 2012,[21] are based on the coupling of triboelectrification and electrostatic induction, which can convert mechanical stimulations into electrical signals.[22] With the advantages of low cost,[23] structural diversity,[24] high output voltage,[25] and multiple working modes,[26] TENGs can serve as both energy-harvesting devices[27−29] and self-powered sensors.[30] Because triboelectrification widely exists in almost all kinds of materials,[31,32] materials with desired elastic moduli can be selected as triboelectric layers to overcome the mechanical mismatch between sensors and attached surfaces. Also, TENGs that served as active sensors[33] can harvest energy from surroundings without an external power source to achieve the ability of self-powering.[34]

Here, a stretchable, skin-friendly, and noninvasive TENG-based wearable sensor for real-time human motion monitoring was fabricated. The deformation of the TENG with a double-layer silicone rubber structure (DS-TENG) resulted in interlayer rubbing because of inhomogeneous strain, producing triboelectric charges that could induce voltage signals in the
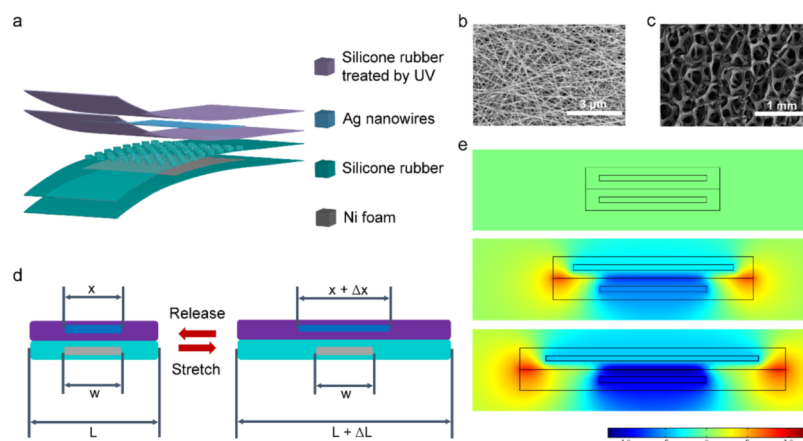
**Figure 1.** Structure and working principle of the DS-TENG. The DS-TENG (a) is composed of silicone rubber and electrodes of AgNWs [SEM in (b), scale bar 3 $\mu$m], Ni foam [SEM in (c), scale bar 1 mm]. (d) Schematic deformation diagram of the DS-TENG and potential simulation by COMSOL (e) to illustrate the working principle.
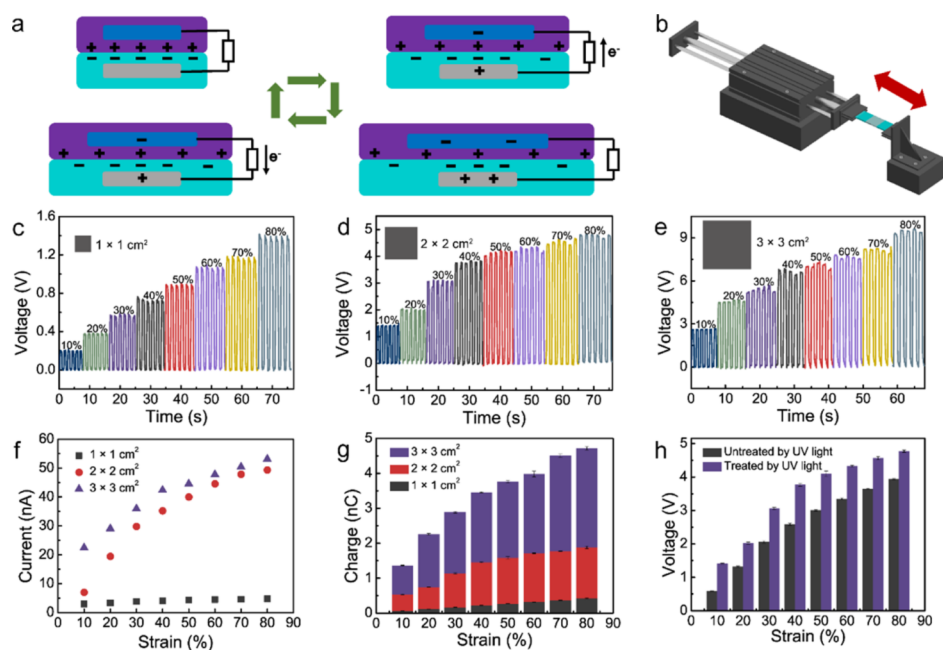


**Figure 2.** Performance of the DS-TENG under stretching. The operation principle and measurement system for stretching testing of the DS-TENG are illustrated in (a,b). The measured open-circuit voltage of DS-TENGs with different electrode sizes (c) 1 × 1, (d) 2 × 2, and (e) 3 × 3 cm² under different stretched strains. The measured (f) short-circuit current and (g) charges with different electrode sizes under different stretched strains. (h) Measured open-circuit voltage of UV-treated and untreated DS-TENGs under different stretched strains.

electrodes in response to the deformation. The voltage outputs of DS-TENG under different conditions were tested. Then, the DS-TENG was demonstrated as a self-powered joint-bending sensor and a three-dimensional muscle sensor (3D muscle sensor), detecting the changes of different areas of the muscle when the body was moving. It was the first time to three-dimensionally characterize the deformation of the muscle using a matrix of DS-TENGs, which showed its promising application perspectives as wearable sensors in modeling human body motion and the human—machine interface.

### ■ RESULT AND DISCUSSION

The structure of the DS-TENG is illustrated in Figure 1. Silver nanowire (AgNW) networks and a Ni foam, which had the same size and were chosen as electrodes, were sandwiched with silicone rubber (Smooth-On, Ecoflex 00-20). Compared to

normal materials, like fluorinated ethylene propylene and nylon, silicone rubber is more stretchable and skin-friendly. The top layer of silicone rubber was treated by UV light for 15 min, whereas the bottom layer of silicone rubber was untreated (Figure 1a). On the basis of different electron affinities of UV-treated and untreated silicone rubber, electrons will transfer from one surface to another when they are in contact. Scanning electron microscopy (SEM) images of the AgNW networks and the Ni foam are shown in Figure 1b,c. Because of the existing networks of the AgNW networks and the Ni foam, silicone rubber could percolate into them and firmly combine with them. Schematic fabrication processes of the DS-TENG are illustrated in Figure S1. Figure 1d reveals the deformation processes of the DS-TENG. The silicone rubber layer with AgNWs was stretchable and bendable, whereas the part embedded with the Ni foam was bendable but nonstretchable. Thus, it could be
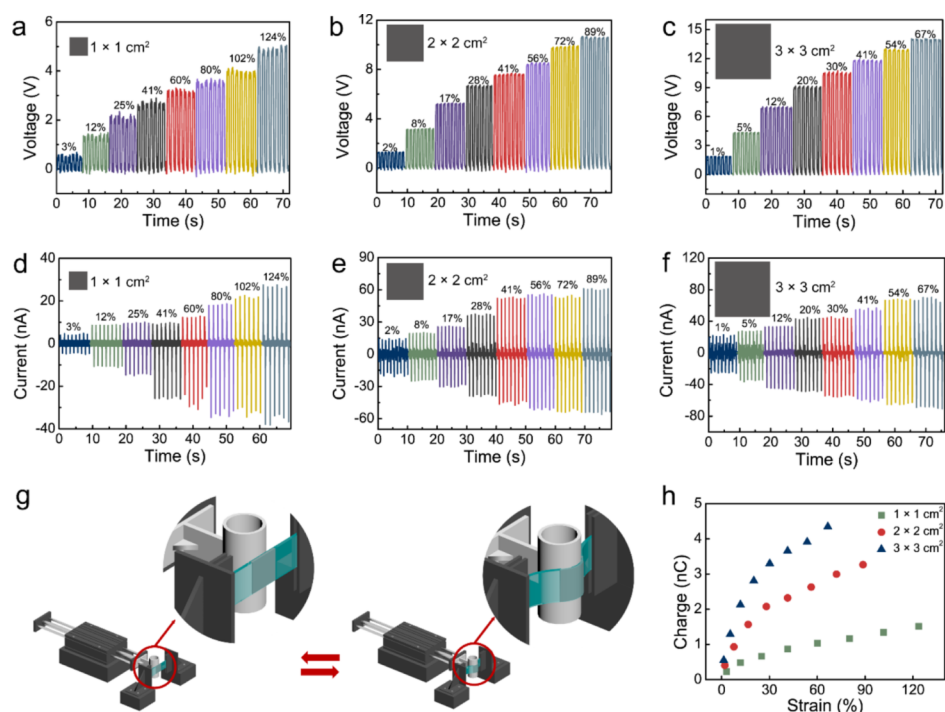
**Figure 3.** Performance of the DS-TENG under extrusion. The measured (a–c) open-circuit voltage and (d–f) short-circuit current of DS-TENGs with different electrode sizes at different levels of extrusion. (g) Schematic diagram of the measurement system for extrusion. (h) Measured transferred charges of DS-TENGs with different electrode widths at different levels of extrusion.

assumed that the top layer of silicone rubber containing the AgNW networks can deform uniformly as usual. On the contrary, the Ni foam embedded with silicone rubber could not be stretched, whereas the DS-TENG was stretched. The initial lengths of the AgNW networks and the Ni foam were denoted as $x$ and $w$ ($x = w$), respectively. The whole length of DS-TENG was denoted as $L$. $\Delta x$ and $\Delta L$ were denoted as the changes of length for the AgNW electrode and the DS-TENG, respectively. When the DS-TENG was stretched to $L + \Delta L$, the length of the AgNW electrode was stretched to $x + \Delta x$ ($\Delta x/x = \Delta L/L$), whereas the length of the Ni foam electrode remained the same as the initial value. When the DS-TENG was released, it recovered to the initial status. The simulation of potential distribution of the DS-TENG by COMSOL is presented in Figure 1e. As the DS-TENG was stretched, the potential difference between the AgNW electrode and the Ni foam electrode would rise simultaneously, which predicted the feasibility of this structure.

The performance and working principles of the DS-TENG are depicted in Figure 2 in detail. Figure 2a illustrates the working principle of the DS-TENG. At the initial status, the Ni foam electrode overlaps with the AgNW electrode. Negative triboelectric charges, uniformly distributed at the interface on the side of the silicone rubber without UV light treating (layer 2), counterpoised the effect of positive charges at the surface on the side of the silicone rubber treated by UV light (layer 1). The AgNW electrode had the same electrical potential as the Ni foam electrode. Once DS-TENG was stretched, the distribution of charges would change because of inhomogeneous strain of different parts, but the total amount of charges remained unchanged. On the surface of layer 1, the charges distributed uniformly with reduced charge density. On the opposite side, the part of layer 2 embedded with the Ni foam electrode could not be stretched and its charge density remained the same as the

initial status. Therefore, it caused the difference of the charge density between the AgNW electrode area and the Ni foam electrode area. Then, the electrons would continuously flow from the Ni foam electrode to the AgNW electrode until DS-TENG's stretch paused. When the DS-TENG was released, the electrons would flow from the AgNW electrode back to the Ni foam electrode. The charge density of silicone rubber except for the area with Ni foam embedded increased gradually until the DS-TENG got back to its initial status. The negative charges of layer 2 were fully counterpoised by the positive charges of layer 1.

The measurement system for stretching the DS-TENG is illustrated in Figure 2b. One side of the DS-TENG was fixed on a linear motor and another side was fixed on a fixed holder. Figure 2c–e shows the measured open-circuit voltage ($V_{oc}$) of DS-TENGs with different electrode sizes ($1 \times 1$, $2 \times 2$ and $3 \times 3$ cm$^2$) under different total strains. As the stretched strain increased, the generated $V_{oc}$ increased obviously in different sizes. When DS-TENGs were stretched under the same strain, the larger the size of the electrodes was, the higher the output voltage was. For one DS-TENG, the output voltages would gradually increase with the increasing of the stretched strain. As shown in Figure 2f,g, the measured short-circuit current ($I_{sc}$) and transferred charges ($Q$) increased gradually as the stretched strain increased, respectively. The DS-TENG with an electrode size of $3 \times 3$ cm$^2$ presented best output performance among all under the same strain. The results showed that the slope of current versus the strain response curve was higher in the small strain region (<40%) than the one in large strain region (>40%). Therefore, the DS-TENG was more sensitive for sensing tiny deformation by small strain. To demonstrate the effect of UV light, Figure 2h shows the measured $V_{oc}$ of DS-TENGs with and without UV light treatment under different stretched strains. Tribo-pairs with one silicone rubber treated by UV light
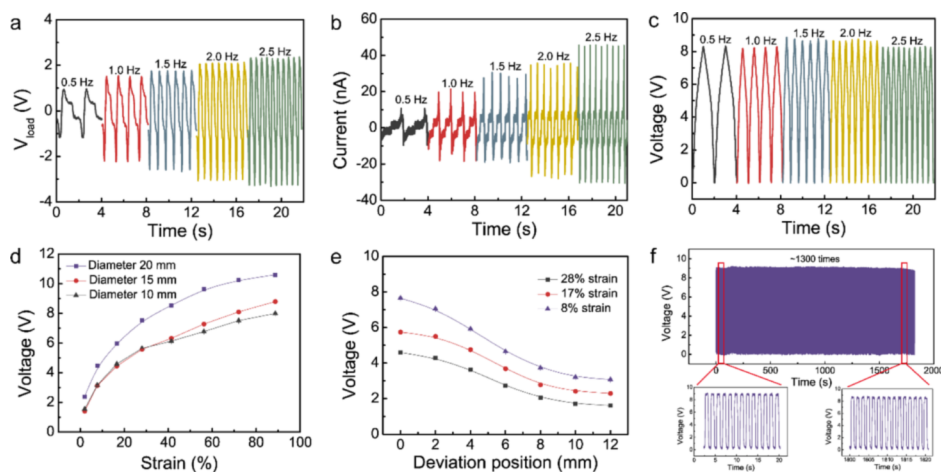
**Figure 4.** Performance characterization of the DS-TENG (electrode size: $2 \times 2$ cm$^2$). (a) Load voltage, (b) short-circuit current, and (c) open-circuit voltage of the DS-TENG under different deformation frequency from 0.5 to 2.5 Hz. (d) Output voltage of DS-TENGs with different diameters under variable deformation degrees. (e) Output voltage of DS-TENGs in the case of three deformation degrees under different deviation distances. (f) Device robustness investigation, and there is no observable performance degradation.
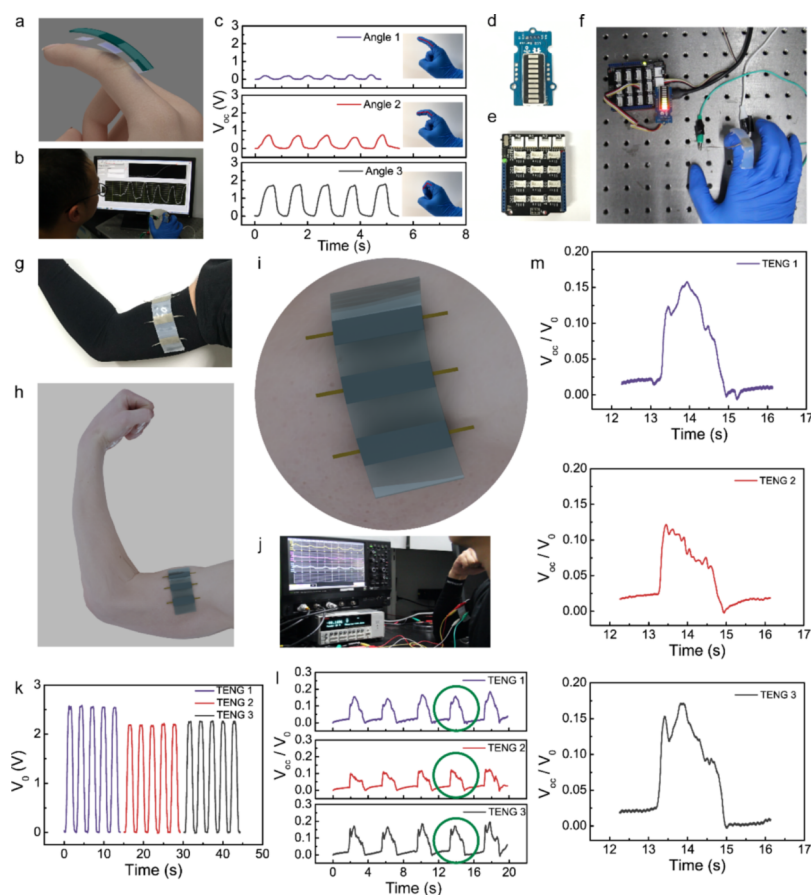


**Figure 5.** Application in self-powered human action sensors. (a) Schematic diagram of the DS-TENG for a human finger. (b) Photo of real-time outputs with one joint bending. (c) Output voltage with one joint bending under different bending angles. (d,e) Circuits for LED bar demonstrating. (f) Photo of LED bar demonstrating under one joint bending sensed by one DS-TENG. (g) Photo of three DS-TENGs' matrix fixed on the muscle. (h,i) Schematic diagram of three DS-TENGs' matrix fixed on the muscle. (j) Photo of three channels' real-time outputs with one arm bending. (k) Output voltage of the three DS-TENGs under the same stretched deformation on the linear motor. (l) Output of the three DS-TENGs sensing different muscle areas at the same time in the case of arm bending. (m) Amplifying signal peaks of the three DS-TENGs sensing different muscle areas.

exhibited better output performance than the untreated situation. In addition, UV light-treated silicone rubber could be stretched more smoothly than the untreated one because of the reduction of viscosity after UV light treatments.

To investigate the performance of DS-TENGs under extrusion, two translation stages with holders and a computer-controlled linear motor were used as shown in Figure 3g. An acrylic pipe (analog to surfaces with different curvatures) was

fixed on the linear motor to extrude the DS-TENG. At the original status, the pipe touched on the surface of the DS-TENG without deformation. Then, under the computer control, the pipe on the linear motor reciprocated within a certain range, which resulted in a certain degree of deformation of the DS-TENG. The measured $V_{oc}$ and $I_{sc}$ of DS-TENGs with different electrode sizes at different levels of extrusion are shown in Figure 3a−f. With the increase of extruding deformation, the electrical output performance of DS-TENGs significantly increased with the same electrode size. It could also be found that the size of the electrode had a greater impact on the output performance of DS-TENGs. Under similar degrees of deformation, the electrode size of $3 \times 3$ cm$^2$ DS-TENG showed the best electrical output performance, whereas the electrode size of $1 \times 1$ cm$^2$ DS-TENG exhibited a relatively lower output performance. Figure 3h shows transferred charges of DS-TENGs with different electrode sizes at extrusion of different levels. At a small degree of deformation, transferred charges significantly increased with the increasing of the deformation degrees, whereas they increased relatively slowly at the large deformation region. Comparing to the stretching deformation shown in Figure 2, extruding deformation of DS-TENGs presented a much more outstanding output performance when they were at the same degree of deformation.

To further investigate the effect of deformation frequency on the DS-TENG, the voltage and current signals were measured at extruding deformation frequencies of 0.5, 1.0, 1.5, 2.0, and 2.5 Hz (Figure 4a−c). For the frequency experiments, the equipment was the same as the previous one. Through changing the kinematic velocity of the linear motor on the computer, different frequencies could be realized. In Figure 4a, load voltage (with a resistance of 100 MΩ) of the DS-TENG increased with the increase of frequency, which meant a high working frequency would enhance the load voltage effectively. The same trend was also found in the short-circuit current shown in Figure 4b. However, in Figure 4c, the open-circuit voltage of the DS-TENG remained almost constant at five different frequencies. Hence, the open-circuit voltage could serve as a reliable signal under the circumstance, where the effect of deformation frequencies needed to be eliminated.

Furthermore, the influence of surface curvature (corresponding to different pipe diameters) and contact position between the acrylic pipe and the DS-TENG on the output performance was studied. Figure 4d shows that $V_{oc}$ of DS-TENGs gradually increased as the deformation degree increased under pipe diameters of 10, 15, and 20 mm. At the same level of deformation degrees, DS-TENGs interacting with a smaller surface curvature (corresponding to acrylic pipes with larger diameters) showed a better output performance. When the degree of deformation was relatively small (<30%), there was no big difference in the output voltage of DS-TENGs interacting with acrylic pipes of different diameters. However, in the large deformation region, the larger the pipe diameter was, the better the output voltage was. As shown in Figure 4e, when DS-TENG interacted with the acrylic pipe, the output voltage decreased gradually as the contacting point deviates further from the center under the same stretched strain. The output voltage decreasing rate was fastest in the range of deviation position from 4 to 8 mm. The output voltage decreasing rate was relatively slower at both the beginning and the end range. A stability test of the DS-TENG over 1300 cycles is shown in Figure 4f. There was no obvious performance degradation. According to the above

analysis, DS-TENG showed great potential for a reliable deformation sensor.

On the basis of the above characterization of DS-TENG, wearable joint and muscle sensors were developed with DS-TENGs. Schematic diagram of the DS-TENG as a joint bending sensor mounted on the index finger of a person is exhibited in Figure 5a. Both ends and the central part (corresponding to the electrodes of the DS-TENG) of the DS-TENG were fixed conformally on the finger. The central part stuck to the joint of the index finger, which could eliminate the disturbance of friction between the finger and the silicone rubber (the parts with electrodes). As presented in Figure 5b, DS-TENG (electrode: $1 \times 1$ cm$^2$; silicone rubber: $1 \times 5$ cm$^2$) was fixed on the finger joint. The device was stretched when the finger bends, whereas it was released when the finger straightened. DS-TENG generated different output voltage signals according to the degrees of finger bending (Video S1). In Figure 5c, DS-TENG mounted on the finger could vividly distinguish different bending angles of the finger joint through different output voltage signals. The open-circuit voltage could reach 2.0 V when the joint totally bent. Even for a small bending angle like angle 1, the output voltage signal around 0.5 V could be easily detected. When the finger bent in different angles, the change of the output voltage could be directly indicated by a light-emitting diode (LED) bar system with different numbers of light-up LEDs (Figure 5f and Video S2), providing a visual monitoring of the state of body motion. The LED bar circuit is shown in Figure 5d,e.

The DS-TENG could also be applied as a muscle sensor for delicately capturing tiny muscle motion, especially for different areas at the same time, which could be useful for modeling human body motion and the human−machine interface. A 3D sensor integrating three DS-TENGs to depict the deformations of different muscle areas was demonstrated. Digital photograph and schematic diagram of the 3D sensor integrating three DS-TENGs fixed on the muscle are vividly exhibited in Figure 5g,h, respectively. The enlarged schematic diagram of the 3D muscle sensor is also illustrated in Figure 5i. As shown, three DS-TENGs were arranged around the muscle at the same spacing. Before being fixed on the muscle, the output voltage of the three DS-TENGs was tested simultaneously on the linear motor with the same degrees of deformation, as shown in Figure 5k. The results turned out that the output voltage of DS-TENG 2 and DS-TENG 3 was about 2.2 V and the output voltage of DS-TENG 1 was about 2.5 V. Then, the sensor with three DS-TENGs was fixed on the muscle conformally. When the arm bent, the profile of the muscle began to change, nonuniformly in different areas. Such complicated nonuniform deformation information could be easily recorded by the 3D muscle sensor with different output voltages at different muscle areas. Thus, the deformation degrees of different muscle areas could be recorded effectively in real time. The real-time testing of the 3D muscle sensor when muscle deformed is shown in Figure 5j and Video S3. In detail, the output voltages of the 3D muscle sensor generated by muscle deformation were depicted in Figure 5l. For reliable comparison, these signals were normalized by the corresponding maximum voltage shown in Figure 5j, respectively. The DS-TENG 3 presented the strongest output signal, which meant the muscle area sensed by the DS-TENG 3 has the largest deformation degree. The deformation degree of the muscle area corresponding to the DS-TENG 1 was slightly smaller than the one sensed by the DS-TENG 3. The deformation degree of the muscle area sensed by the DS-

TENG 2 was the smallest. The detailed information of single cycle muscle movement could be clearly seen in Figure 5m after enlarging a single signal of three DS-TENGs. The signal shape of three DS-TENGs on the muscle demonstrated totally different, especially peak shapes, which represented that the DS-TENG could meticulously exhibit the deformation of different muscle areas. On the basis of the above principle, the density of DS-TENGs could be greatly enhanced for more precise measurements. The ability of DS-TENGs to sense the variation of complex surfaces like the human body could provide great potential applications in the areas of soft robots, daily health monitoring, virtual reality, and so on.

## CONCLUSIONS

In this paper, a stretchable, skin-friendly, and noninvasive TENG-based wearable sensor for real-time human motion monitoring is presented. With a double-layer silicone rubber structure and electrodes with different stretchabilities, the deformation of the DS-TENG results in interlayer rubbing because of inhomogeneous strain, producing triboelectric charges that can induce voltage signals in the electrodes in response to the deformation. The size of the electrode, different deformation types ,and other crucial factors which can influence the output performance of the DS-TENG were thoroughly studied. Then, a joint-bending sensor based on the DS-TENG was demonstrated, which could generate different output voltage signals according to the bending degrees of the joint, and a visual system with different numbers of LED lighted up on an LED bar according to the finger-bending angle was also shown. Furthermore, a DS-TENG matrix was fabricated to serve as a 3D muscle sensor. The output voltages of the DS-TENGs could be simultaneously monitored to reflect the deformation degrees of different muscle areas, applicable in modeling human body motion and the human−machine interface. The work provides a promising design for new types of self-powered wearable electronics in the future.

## EXPERIMENTAL SECTION

**Fabrication of the DS-TENG.** For one part of the DS-TENG, the AgNW solution, purchased from Nanjing XFNANO Materials Tech Co. Ltd., was dropped onto an acrylic plate patterned with Kapton tapes for desired shapes. The Kapton tapes were removed after the AgNW solution was dried in room temperature. Silicone rubber (Smooth-On, Ecoflex 00-20) with part A and part B was mixed in a 1:1 weight ratio. Then, the silicone rubber mixture was covered onto the AgNWs. After curing at room temperature for at least 5 h, the silicone rubber, some totally permeated into the AgNW network, was peeled off from the acrylic plate. The AgNW network forms an electrode. Then, the AgNW electrode was attached by a conducting tape and sealed by additional silicone rubber, which is not cured. After curing for at least 5 h, the silicone rubber, with the AgNW electrode, was peeled off from acrylic mold. After that, both sides of the silicone rubber were treated by UV light for about 15 min.

For another part of the DS-TENG, silicone rubber was poured into the acrylic mold with cylindric microprisms in the middle. When the silicone rubber was not totally curing, the Ni foam electrode was put on it. The Ni foam was a 3D nickel network with macroporous foam-like structure (thickness = 0.3 mm, surface density = 350 g/m$^2$, poriness = 98%). It was purchased from Kunshan GuangJiaYuan New Materials Co. Ltd.. After the silicone rubber was totally cured, the Ni foam electrode was attached by the conducting tape and sealed by additional silicone rubber, which is not cured. After curing for at least 5 h, the silicone rubber embedded by the Ni foam was peeled off from the acrylic mold. A cylindrical microprism could increase the roughness of the surface to enhance the friction between two triboelectric layers. The

cylindrical microprism was 1 mm in diameter and 1 mm in height. They were arranged in the form of a square with a space of 1 mm. In the end, the silicone rubbers embedded with the AgNW electrode and the Ni foam electrode were stacked together. Both ends were glued by silicone rubber to form the DS-TENG. The thickness of the silicon rubber covering the AgNW electrode from the lower side was about 1 mm and that covering the Ni foam from the upper side was about 2 mm, including a cylindrical microprism of 1 mm height. As the thickness of the dielectric would affect the output,[35] the thickness of the silicon rubber in this work was kept the same.

**Characterization and Measurement.** SEM images of AgNW networks and Ni foam were characterized by a Nova NanoSEM 450. The electric output performance of the DS-TENG was measured by two Keithley 6514 electrometers and one Keithley 6517 electrometer. DS-TENG-based muscle sensor was recorded by an oscilloscope (Teledyne LeCroy HD 4096) and a data acquisition hardware (PowerLab 4/35).

## ASSOCIATED CONTENT

**Ⓢ Supporting Information**

The Supporting Information is available free of charge on the ACS Publications website at DOI: 10.1021/acsami.9b12195.

Fabrication process of the DE-TENG, schematic diagram of DS-TENG under extrusion on the linear motor, and original output voltage of three DS-TENGs sensing different muscle areas at the same time in the case of arm bending (PDF)

DS-TENG for one joint bending sensing (MP4)

LED bar demonstrating under one joint bending with the DS-TENG (MP4)

Three DS-TENGs' matrix for different areas of muscle sensing at the same time (MP4)

## AUTHOR INFORMATION

**Corresponding Author**
*E-mail: zhong.wang@mse.gatech.edu.

**ORCID** ⓘ
Zhong Lin Wang: 0000-0002-5530-0380

**Author Contributions**
‖H.W., D.L., and W.Z. contributed equally.

**Notes**
The authors declare no competing financial interest.

## ACKNOWLEDGMENTS

## REFERENCES

(1) Hong, S.; Lee, H.; Lee, J.; Kwon, J.; Han, S.; Suh, Y. D.; Cho, H.; Shin, J.; Yeo, J.; Ko, S. H. Highly Stretchable and Transparent Metal Nanowire Heater for Wearable Electronics Applications. *Adv. Mater.* **2015**, 27, 4744−4751.

(2) Lee, S.; Shin, S.; Lee, S.; Seo, J.; Lee, J.; Son, S.; Cho, H. J.; Algadi, H.; Al-Sayari, S.; Kim, D. E.; Lee, T. Ag Nanowire Reinforced Highly Stretchable Conductive Fibers for Wearable Electronics. *Adv. Funct. Mater.* **2015**, 25, 3114−3121.

(3) Li, W.; Torres, D.; Wang, T.; Wang, C.; Sepúlveda, N. Flexible and Biocompatible Polypropylene Ferroelectret Nanogenerator (FENG):

on the Path toward Wearable Devices Powered by Human Motion. *Nano Energy* **2016**, *30*, 649−657.

(4) Zeng, W.; Shu, L.; Li, Q.; Chen, S.; Wang, F.; Tao, X.-M. Fiber-based Wearable Electronics: a Review of Materials, Fabrication, Devices, and Applications. *Adv. Mater.* **2014**, *26*, 5310−5336.

(5) Xu, J.; Wang, S.; Wang, G.-J. N.; Zhu, C.; Luo, S.; Jin, L.; Gu, X.; Chen, S.; Feig, V. R.; To, J. W. F.; Rondeau-Gagné, S.; Park, J.; Schroeder, B. C.; Lu, C.; Oh, J. Y.; Wang, Y.; Kim, Y.-H.; Yan, H.; Sinclair, R.; Zhou, D.; Xue, G.; Murmann, B.; Linder, C.; Cai, W.; Tok, J. B.-H.; Chung, J. W.; Bao, Z. Highly Stretchable Polymer Semiconductor Films through the Nanoconfinement Effect. *Science* **2017**, *355*, 59−64.

(6) Ouyang, H.; Liu, Z.; Li, N.; Shi, B.; Zou, Y.; Xie, F.; Ma, Y.; Li, Z.; Li, H.; Zheng, Q.; et al. Symbiotic Cardiac Pacemaker. *Nat. Commun.* **2019**, *10*, 1821.

(7) Meng, K.; Chen, J.; Li, X.; Wu, Y.; Fan, W.; Zhou, Z.; He, Q.; Wang, X.; Fan, X.; Zhang, Y.; et al. Flexible Weaving Constructed Self-Powered Pressure Sensor Enabling Continuous Diagnosis of Cardiovascular Disease and Measurement of Cuffless Blood Pressure. *Adv. Funct. Mater.* **2019**, *29*, 1806388.

(8) Lai, Y.-C.; Deng, J.; Liu, R.; Hsiao, Y.-C.; Zhang, S. L.; Peng, W.; Wu, H.-M.; Wang, X.; Wang, Z. L. Actively Perceiving and Responsive Soft Robots Enabled by Self-Powered, Highly Extensible, and Highly Sensitive Triboelectric Proximity-and Pressure-Sensing Skins. *Adv. Mater.* **2018**, *30*, 1801114.

(9) Marín-Morales, J.; Higuera-Trujillo, J. L.; Greco, A.; Guixeres, J.; Llinares, C.; Scilingo, E. P.; Alcañiz, M.; Valenza, G. Affective Computing in Virtual Reality: Emotion Recognition from Brain and Heartbeat Dynamics Using Wearable Sensors. *Sci. Rep.* **2018**, *8*, 13657.

(10) Hong, G.; Lieber, C. M. Novel Electrode Technologies for Neural Recordings. *Nat. Rev. Neurosci.* **2019**, *20*, 330−345.

(11) Kozai, T. D. Y.; Jaquins-Gerstl, A. S.; Vazquez, A. L.; Michael, A. C.; Cui, X. T. Brain Tissue Responses to Neural Implants Impact Signal Sensitivity and Intervention Strategies. *ACS Chem. Neurosci.* **2015**, *6*, 48−67.

(12) Stoppa, M.; Chiolerio, A. Wearable Electronics and Smart Textiles: a Critical Review. *Sensors* **2014**, *14*, 11957−11992.

(13) Kim, K.; Choi, J.-Y.; Kim, T.; Cho, S.-H.; Chung, H.-J. A Role for Graphene in Silicon-based Semiconductor Devices. *Nature* **2011**, *479*, 338.

(14) Vivien, L.; Osmond, J.; Fédéli, J.-M.; Marris-Morini, D.; Crozat, P.; Damlencourt, J.-F.; Cassan, E.; Lecunff, Y.; Laval, S. 42 GHz Pin Germanium Photodetector Integrated in a Silicon-on-Insulator Waveguide. *Opt. Express* **2009**, *17*, 6252−6257.

(15) Shi, J.; Fang, Y. Flexible and Implantable Microelectrodes for Chronically Stable Neural Interfaces. *Adv. Mater.* **2018**, 1804895.

(16) Lind, G.; Linsmeier, C. E.; Thelin, J.; Schouenborg, J. Gelatine-embedded Electrodes—a Novel Biocompatible Vehicle Allowing Implantation of Highly Flexible Microelectrodes. *J. Neural Eng.* **2010**, *7*, 046005.

(17) Ren, J.; Zhang, Y.; Bai, W.; Chen, X.; Zhang, Z.; Fang, X.; Weng, W.; Wang, Y.; Peng, H. Elastic and Wearable Wire-Shaped Lithium-ion Battery with High Electrochemical Performance. *Angew. Chem., Int. Ed.* **2014**, *53*, 7864−7869.

(18) Kou, L.; Huang, T.; Zheng, B.; Han, Y.; Zhao, X.; Gopalsamy, K.; Sun, H.; Gao, C. Coaxial Wet-Spun Yarn Supercapacitors for High-Energy Density and Safe Wearable Electronics. *Nat. Commun.* **2014**, *5*, 3754.

(19) Jost, K.; Stenger, D.; Perez, C. R.; McDonough, J. K.; Lian, K.; Gogotsi, Y.; Dion, G. Knitted and Screen Printed Carbon-Fiber Supercapacitors for Applications in Wearable Electronics. *Energy Environ. Sci.* **2013**, *6*, 2698−2705.

(20) He, X.; Zou, H.; Geng, Z.; Wang, X.; Ding, W.; Hu, F.; Zi, Y.; Xu, C.; Zhang, S. L.; Yu, H.; Xu, M.; Zhang, W.; Lu, C.; Wang, Z. L. A Hierarchically Nanostructured Cellulose Fiber-Based Triboelectric Nanogenerator for Self-Powered Healthcare Products. *Adv. Funct. Mater.* **2018**, *28*, 1805540.

(21) Fan, F.-R.; Tian, Z.-Q.; Wang, Z. L. Flexible Triboelectric Generator. *Nano Energy* **2012**, *1*, 328−334.

(22) Wang, Z. L. Triboelectric Nanogenerators as New Energy Technology for Self-Powered Systems and as Active Mechanical and Chemical Sensors. *ACS Nano* **2013**, *7*, 9533−9557.

(23) Yang, Y.; Zhu, G.; Zhang, H.; Chen, J.; Zhong, X.; Lin, Z.-H.; Su, Y.; Bai, P.; Wen, X.; Wang, Z. L. Triboelectric Nanogenerator for Harvesting Wind Energy and as Self-Powered Wind Vector Sensor System. *ACS Nano* **2013**, *7*, 9461−9468.

(24) Ding, W.; Wang, A. C.; Wu, C.; Guo, H.; Wang, Z. L. Human−Machine Interfacing Enabled by Triboelectric Nanogenerators and Tribotronics. *Adv. Mater. Technol.* **2019**, *4*, 1800487.

(25) Nie, J.; Chen, X.; Wang, Z. L. Electrically Responsive Materials and Devices Directly Driven by the High Voltage of Triboelectric Nanogenerators. *Adv. Funct. Mater.* **2018**, 1806351.

(26) Wu, C.; Wang, A. C.; Ding, W.; Guo, H.; Wang, Z. L. Triboelectric Nanogenerator: A Foundation of the Energy for the New Era. *Adv. Energy Mater.* **2019**, *9*, 1802906.

(27) Zhong, W.; Xu, L.; Yang, X.; Tang, W.; Shao, J.; Chen, B.; Wang, Z. L. Open-Book-Like Triboelectric Nanogenerators Based on Low-Frequency Roll-Swing Oscillator for Wave Energy Harvesting. *Nanoscale* **2019**, *11*, 7199−7208.

(28) Yang, X.; Xu, L.; Lin, P.; Zhong, W.; Bai, Y.; Luo, J.; Chen, J.; Wang, Z. L. Macroscopic Self-Assembly Network of Encapsulated High-Performance Triboelectric Nanogenerators for Water Wave Energy Harvesting. *Nano Energy* **2019**, *60*, 404−412.

(29) Wang, Z. L.; Jiang, T.; Xu, L. Toward the Blue Energy Dream by Triboelectric Nanogenerator Networks. *Nano Energy* **2017**, *39*, 9−23.

(30) Pu, X.; Guo, H.; Chen, J.; Wang, X.; Xi, Y.; Hu, C.; Wang, Z. L. Eye Motion Triggered Self-Powered Mechnosensational Communication System Using Triboelectric Nanogenerator. *Sci. Adv.* **2017**, *3*, No. e1700694.

(31) Nie, J.; Wang, Z.; Ren, Z.; Li, S.; Chen, X.; Wang, Z. L. Power Generation from the Interaction of a Liquid Droplet and a Liquid Membrane. *Nat. Commun.* **2019**, *10*, 2264.

(32) Zou, H.; Zhang, Y.; Guo, L.; Wang, P.; He, X.; Dai, G.; Zheng, H.; Chen, C.; Wang, A. C.; Xu, C. Quantifying the Triboelectric Series. *Nat. Commun.* **2019**, *10*, 1427.

(33) Wang, S.; Lin, L.; Wang, Z. L. Triboelectric Nanogenerators as Self-Powered Active Sensors. *Nano Energy* **2015**, *11*, 436−462.

(34) Wang, Z. L. Self-Powered Nanosensors and Nanosystems. *Adv. Mater.* **2012**, *24*, 280−285.

(35) Niu, S.; Liu, Y.; Wang, S.; Lin, L.; Zhou, Y. S.; Hu, Y.; Wang, Z. L. Theory of Sliding-Mode Triboelectric Nanogenerators. *Adv. Mater.* **2013**, *25*, 6184−6193.